

## Explicit complex time integrators for stiff problems.

Jithin D. George\*, Julian Koellermeier , Samuel Y. Jung\*, and Niall M. Mangan\*

**Abstract.** Most numerical methods for time integration use real-valued time steps. Complex time steps, however, can provide an additional degree of freedom, as we can select the magnitude of the time step in both the real and imaginary directions. We show that specific paths in the complex time plane lead to expanded stability regions, providing clear computational advantages for complex-valued systems. In particular, we highlight the Schrödinger equation, for which complex time integrators can be uniquely optimal. Furthermore, we demonstrate that these benefits extend to certain classes of real-valued stiff systems by coupling complex time steps with the Projective Integration method.

**Key words.** complex time steps, complex time integrators , absolute stability , Schrodinger equation, Projective Integration

**AMS subject classifications.** 30-08, 65E05, 65L05, 65L04, 65M12, 65M20

**1. Introduction.** The complex plane has often been employed to solve real-world problems. Two direct examples are the solution of complicated real-valued integrals via contour integrals [1] and the usage of the intuition gained from poles in the complex plane in control-theory applications [2]. The complex plane provides new insights to real problems, allowing mathematicians to impact practical applications. However, most methods for numerically solving differential equations from time  $a$  to time  $b$  construct a path utilizing only the real line. Here, we highlight particular cases where stepping into the complex plane provides advantages for numerical time integration.

The idea of taking complex time steps is not new. Early work on time stepping in the complex plane focused on systematically avoiding singularities during numerical integration of singular differential equations [3]. Complex time steps have also been used in operator splitting schemes. One of the earliest works in this field is [4], where complex substeps were used to avoid negative and unstable substeps, significantly reducing the truncation error. Following this, complex time steps and complex coefficients have been incorporated into operator splitting methods for various parabolic and nonlinear evolution problems [5, 6, 7, 8, 9, 10, 11, 12]. Complex coefficients have been used for higher order methods for linear systems [13, 14] and in stiff differential algebraic systems [15]. More recently, [16] used Cauchy's integral formula as inspiration to introduce a general framework for deriving integrators using interpolating polynomials in the complex plane. This results in parallel Backward Differentiation Formula (BDF) methods with improved stability regions.

The current paper builds on ideas introduced in [17] and focuses on complex time integrators in the context of stiff problems. These stiff problems often result in bounded stability regions for time integration schemes. We show that the additional dimension offered by complex time steps allows to tune stability regions and design explicit time integrators with significantly enhanced stability properties.

---

\*Department of Engineering Sciences and Applied Mathematics, Northwestern University, Evanston, IL.  
(jithindgeorge93@gmail.com, samyjung@outlook.com, niallmm@gmail.com)

Our paper is organized as follows: In Section 2, we illustrate how to use complex time steps to create customized stability regions and recreate the stability regions of the Runge-Kutta-2 and Runge-Kutta-3 methods using complex Forward Euler time steps. Section 3 explores asymmetric stability regions, a unique property of complex time integrators. We show that the asymmetric stability regions generated by complex time integrators are optimal for complex-valued systems like the nonlinear Schrödinger equation, and highlight a factor of 2 reduction in computational time for the same accuracy. Finally, in Section 4, we combine complex time steps with the Projective Integration method [18, 19, 20, 21] to tackle large spectral gaps in stiff systems with eigenvalues that lie off the real axis.

The code to reproduce the numerical experiments in this paper is available on GitHub <sup>1</sup>.

**2. Expanded regions of stability with complex time-steps.** In this section, we illustrate how complex time steps can be leveraged in numerical time integrators to expand the region of absolute stability. Consider the scalar Dahlquist test problem [22] with parameter  $\lambda \in \mathbb{C}$  given in Equation (2.1).

$$(2.1) \quad \dot{y} = \lambda y, \quad y(0) = y_0.$$

Equation (2.1) can be integrated with a desired time integrator to obtain the following numerical solution after one time step  $\Delta t \in \mathbb{R}_+$ .

$$(2.2) \quad y(t + \Delta t) = \Phi(\lambda \Delta t) y(t),$$

where  $\Phi(z)$  is the stability function of the integrator [23]. The region  $z \in \mathbb{C}$  where  $|\Phi(z)| \leq 1$  is the region of absolute stability for the integrator. For the 1-step first-order Forward Euler (FE) method, the 2-step second-order RK2 method and the 3-step third-order RK3 method, the stability regions are given by Equations (2.3), (2.4) and (2.5), respectively.

$$(2.3) \quad \Phi_{FE}(z) = 1 + z,$$

$$(2.4) \quad \Phi_{RK2}(z) = 1 + z + \frac{z^2}{2},$$

$$(2.5) \quad \Phi_{RK3}(z) = 1 + z + \frac{z^2}{2} + \frac{z^3}{3!}.$$

The stability regions of the FE, RK2, and RK3 methods are shown in Figure 1 (left).

Now, instead of real time steps, we consider integrating Equation (2.1) using a composition of Forward Euler steps with complex time increments. Specifically, we apply up to three successive Forward Euler sub-steps with step sizes  $w_1 \Delta t$ ,  $w_2 \Delta t$ , and  $w_3 \Delta t$ , where  $w_i \in \mathbb{C}$ . The stability polynomial of this 3-step complex Forward Euler (cFE) method is given by

$$(2.6) \quad \Phi_{cFE}(z) = (1 + w_1 z)(1 + w_2 z)(1 + w_3 z)$$

$$(2.7) \quad = 1 + (w_1 + w_2 + w_3)z + (w_1 w_2 + w_2 w_3 + w_1 w_3)z^2 + w_1 w_2 w_3 z^3.$$

By picking certain complex values of  $w_1, w_2, w_3$  in (2.7), we can tailor the stability region of the cFE integrator in (2.7) to be the same as that of FE in (2.3), RK2 in (2.4), or RK3 in

---

<sup>1</sup>[https://github.com/Dirivian/complex\\_time\\_integrators](https://github.com/Dirivian/complex_time_integrators)

(2.5). Each choice of  $w_1, w_2, w_3$  represents a different path from  $t \in \mathbb{R}$  to  $t + \Delta t \in \mathbb{R}$  through the complex time plane. We highlight three different choices, sketched also in Figure 1 (right):

1.  $w_1 = 1, (w_2, w_3 = 0)$ , leading to the 1-step first-order complex Euler method (cFE1).
2.  $w_1 = \frac{1}{2} + \frac{1}{2}i, w_2 = \frac{1}{2} - \frac{1}{2}i, (w_3 = 0)$ , leading to the 2-step second-order complex Euler method (cFE2).
3.  $w_1 \approx 0.186731 + 0.480774i, w_2 \approx 0.626538, w_3 \approx 0.186731 - 0.480774i$ , leading to the 3-step third-order complex Euler method (cFE3).

The corresponding stability regions in Figure 1 (right) recreate the well-known stability regions obtained for the Forward Euler (2.3), RK2 (2.4) and RK3 (2.5) methods.

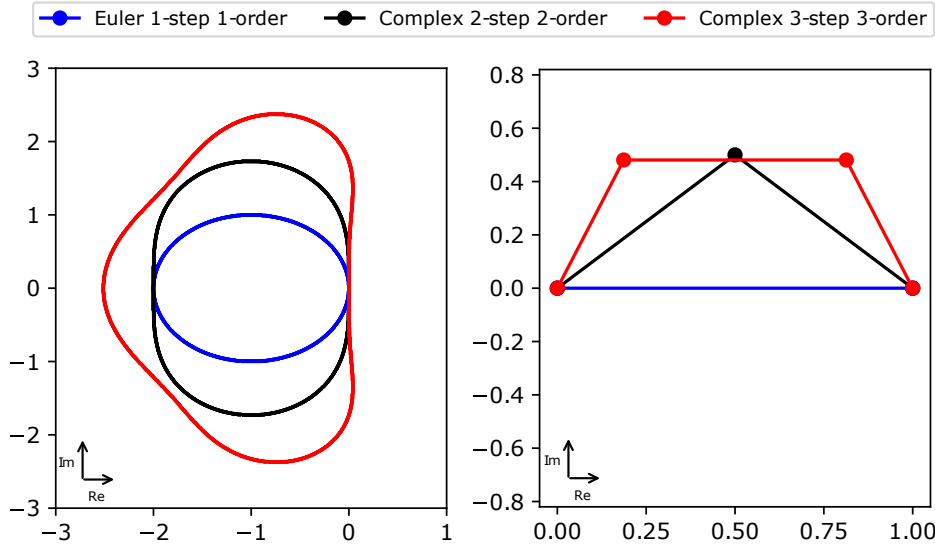


**Figure 1.** Three different complex time-stepping paths (right). The 1-step first-order cFE1, 2-step second-order cFE2 and 3-step third-order cFE3 methods share the same stability regions as the FE (2.3), RK2 (2.4) and RK3 (2.5) methods (left).

Since the paths in Figure 1 (right) have the same stability polynomials as the corresponding FE, RK2, and RK3 methods, they also have the same order of accuracy for linear differential equations. Note that the paths sketched in Figure 1 (right) are not the only ones. In Figure 2, all six 3-step 3rd order paths (for linear differential equations) are shown along with the two 2-step 2nd order paths and the single step forward Euler path. Previous work [14, 13] has demonstrated that appropriately chosen complex time steps can increase the order of accuracy for linear differential equations. Here, however, our focus is on the stability properties of such complex time integrators.

Equation (2.7) suggests the possibility of trading second-order and third-order accuracy in order to obtain customized stability regions. Note, however, that first-order accuracy is necessary to obtain a consistent numerical solution after a total time step of  $\Delta t \in \mathbb{R}$ . In Figure 3, we illustrate a 3-step second-order Forward Euler method (cFE3-2)(blue) and 3-step first-order Forward Euler method (cFE3-1) (yellow) with expanded stability along the negative real axis compared to the 3-step third-order Forward Euler method (cFE3) (red). Note that

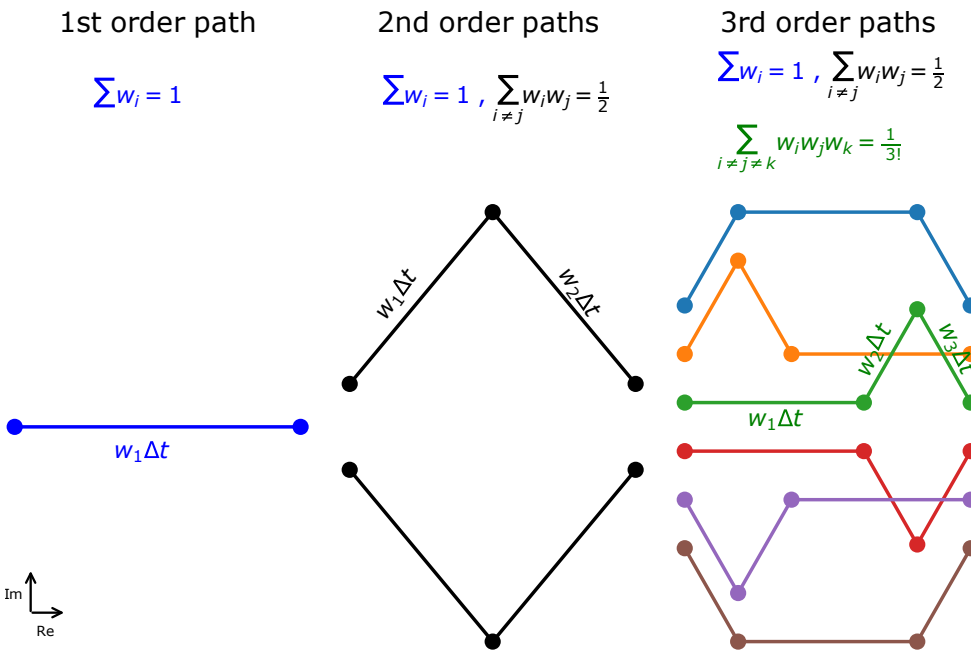


**Figure 2.** All possible 1-step first-order, 2-step second-order, and 3-step third-order complex Forward Euler methods for linear differential equations.

the cFE3-1 method is achieved through purely real time steps.

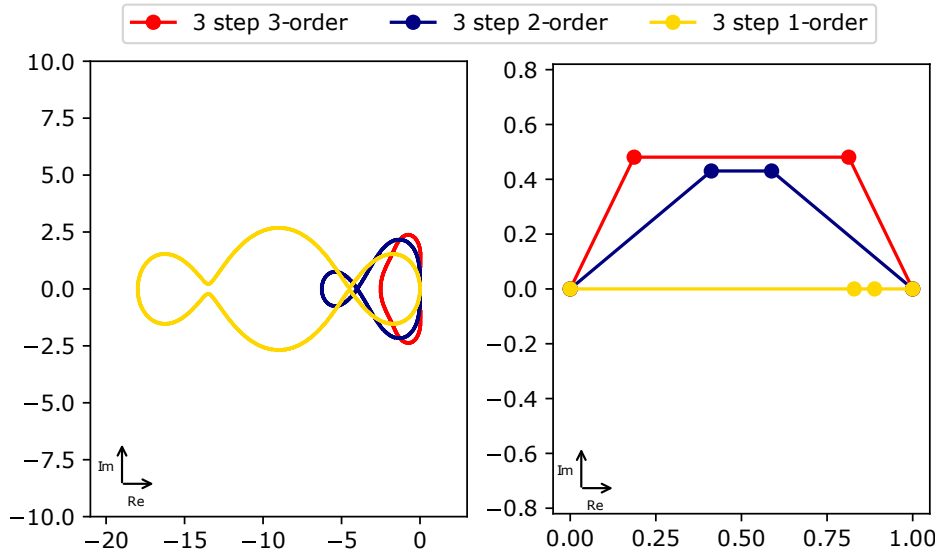


**Figure 3.** By sacrificing accuracy, the stability region can be expanded (left) using complex time steps, as demonstrated by these optimized 3-step complex Euler paths (right) with third-order (cFE3), second-order (cFE3-2), and first-order (cFE3-1) accuracy.

The idea that the order of accuracy can be sacrificed for enhanced stability is not new. Expanded stability regions have been studied in the context of Runge-Kutta methods with real-valued coefficients, where the order of accuracy is sacrificed to obtain a larger stability region [24, 25, 26, 27, 28, 29, 30]. For problems with purely real or purely imaginary eigenvalues, the optimal stability functions/polynomials have been long-studied [24, 27, 26]. In the past decade, Ketcheson and co-authors [29, 30, 28] have explored optimal stability functions in the context of systems  $\dot{y} = Ly$ , where  $y \in \mathbb{R}^n$  and  $L \in \mathbb{R}^{n \times n}$  is a matrix with arbitrary spectrum. In [28], Ketcheson and Ahmadia describe an optimization algorithm to obtain the optimal stability polynomial that allows the maximal time step depending on the spectrum of  $L$ . This algorithm called RKOpt [31] is publicly available through Nodepy [32]. However, the extension of this technique to complex time steps is currently missing.

To our knowledge, this work is the first to use complex time steps to tailor stability polynomials. At first glance, the advantages of complex time integration over traditional real-valued Runge-Kutta methods may not be obvious, particularly given the additional cost of complex arithmetic. Moreover, not all real-valued nonlinear differential equations admit natural extensions into the complex plane. Nevertheless, our approach provides clear benefits in several contexts commonly encountered in applications, such as systems with asymmetric eigenvalue spectra, complex-valued quantum dynamics, and stiff problems with spectral gaps.

The following sections describe how tailored complex time integration enables larger time steps, expands stability regions, and improves computational efficiency. The next section highlights the benefit of asymmetric stability regions which are inaccessible to traditional real-valued integrators but achievable with complex time steps.

**3. Asymmetrically expanded regions of stability.** Complex time integration offers unique stability advantages for problems with complex-valued solutions. Consider the complex-valued Kohn-Sham equations which describe ultra-fast electron dynamics and are known to require extremely small time steps for stability when using standard explicit Runge-Kutta methods [33]. There is an ongoing and active search for efficient time integration techniques with large stable time steps [34, 35, 36] for the simulation of quantum systems. Kononov *et al.* [36] review a number of numerical methods for the simulation of electron dynamics using the complex-valued Kohn-Sham equations. Given the expense of implicit methods, they express a specific need for explicit methods with expanded stability regions. Complex time integrators can help fill this gap since they incur minimal additional cost for complex-valued problems and can potentially reduce computational effort by expanding stability regions to allow for larger time-steps.

In this section, we explore a unique feature of complex time integration: asymmetric stability regions. Complex time steps can result in stability polynomials with complex valued coefficients. The associated stability regions can then be asymmetric about the real axis, a feature that is not present for real-valued coefficients. For real-valued problems, this asymmetry can be disadvantageous since the eigenvalues of real-valued problems appear as complex conjugate pairs symmetric about the real axis. In contrast, for complex-valued problems which have asymmetric eigenvalue spectra, complex coefficients can yield substantially larger stability regions in the relevant direction.

To demonstrate these ideas, we first consider a generic example, followed by simulations

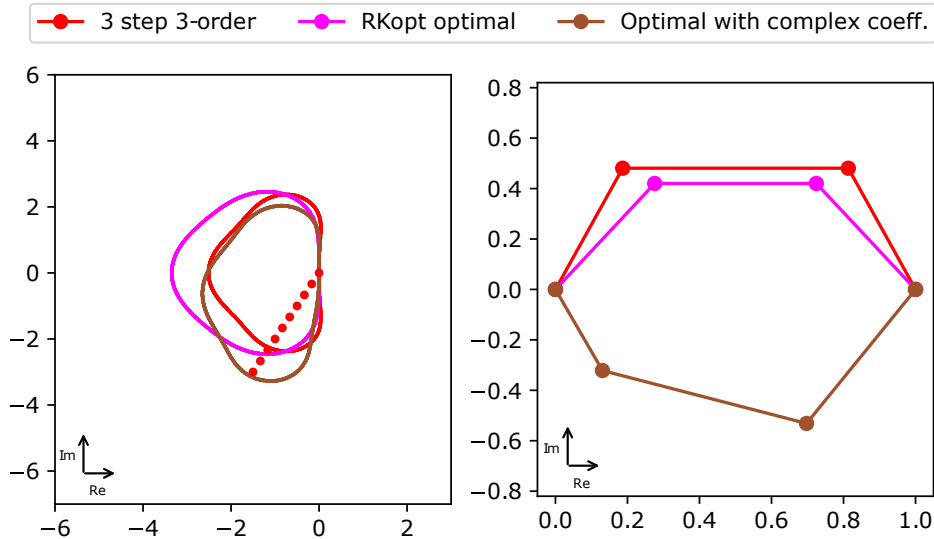


**Figure 4.** Complex coefficients in optimal stability polynomials often result in asymmetrical stability regions. The 3-step third-order (cFE3) complex integrator (red curves) is not optimal for the eigenvalues (red dots, left panel). RKOpt [31] yields the stability polynomial in Eq. (3.1), corresponding to the optimal 3-stage second-order real integrator (magenta curves). An optimized 3-stage complex integrator (brown curves) achieves the stability polynomial in Eq. (3.2) which allows the largest possible time steps for these eigenvalues.

of the linear and nonlinear Schrödinger equations as illustrative application problems.

**3.1. A simple example.** Consider the linear system  $\dot{y} = Ay$  for  $A \in \mathbb{R}^{n \times n}$  with eigenvalues visualized by the red dots in Figure 4 (left). The naive 3-step 3rd order complex integrator cFE3 from the previous section (resulting in the stability domain bounded by the red curve) is obviously not optimally designed and would force a small time step size.

The magenta curve in Figure 4 (left) sketches the better but still symmetric stability region of the stability polynomial given by

$$(3.1) \quad \Phi(z) = 1 + z + \frac{z^2}{2} + 0.1134z^3,$$

which is the optimal stability polynomial with real-coefficients for a 3-stage second-order method obtained using RKOpt [31] for these eigenvalues.

As discussed in the previous section, we can recreate this stability region using three complex Forward Euler steps, leading to the magenta path in Figure 4 (right). We can also choose three complex time steps such that the stability polynomial has complex-valued coefficients. This allows us to numerically find the better stability polynomials. The particular choice of  $w_1 \approx 0.1306 - 0.3217i$ ,  $w_2 \approx 0.5667 - 0.2097i$ ,  $w_3 \approx 0.3027 + 0.5314i$  leads to the stability polynomial in Equation (3.2), visualized in Figure 4 by the brown curve.

$$(3.2) \quad \Phi(z) = 1 + z + \frac{z^2}{2} + (0.1134 - 0.06i)z^3.$$

The brown curve clearly demonstrates the advantage of complex time integration. The 3-step 2nd order complex integrator produces an asymmetric stability region that fully encompasses the relevant eigenvalues of the system (red dots), allowing larger stable time steps for the same spectrum compared to the 3-stage 2nd order integrator with real coefficients. This illustrates that complex coefficients can be used to expand the stability region in the directions where it is most needed, rather than being constrained by symmetry requirements as in the real-valued case.

We note that the 3-stage 2nd order optimized real integrator remains the optimal choice if one has to take time steps along both these eigenvalues and their complex conjugates, as occurs in real-valued systems with complex conjugated pairs of eigenvalues. Overall, these results illustrate that complex time integration combined with optimized stability polynomials provides a clear benefit for problems with asymmetric complex eigenvalue spectra, enabling larger stable time steps and more efficient simulations.

**3.2. Optimally stable integrators for the Schrodinger equation.** To demonstrate the expanded stability benefits of complex time steps on a practical system, we consider a classical complex-valued problem: the linear Schrodinger equation [37] given by Equation (3.3),

$$(3.3) \quad iu_t + \frac{1}{2}u_{xx} = 0.$$

For typical space discretizations, the linear Schrodinger equation has eigenvalues  $\lambda_i \in \mathbb{C}$  along the negative imaginary axis (see Figure 5). We show that for systems with all eigenvalues on either the positive or negative imaginary axis, the optimal first-order 2-stage integrator i.e the first-order 2-stage integrator that allows the maximal stable time step size, must have complex coefficients.

**Theorem 3.1.** *For a linear system  $\dot{y} = Ay$ , where  $y \in \mathbb{R}^n$  and  $A \in \mathbb{R}^{n \times n}$  is a matrix whose eigenvalues  $\lambda \in \mathbb{C} \setminus \mathbb{R}$  lie entirely on either the positive imaginary axis, i.e.,  $\lambda = +i|\lambda|$ , or the negative imaginary axis, i.e.,  $\lambda = -i|\lambda|$ , the optimal stability polynomial for a 2-stage first-order integrator has complex coefficients.*

*Proof.* Without loss of generality, consider a system  $\dot{y} = Ay$  with all the eigenvalues  $\lambda$  of  $A$  on the positive imaginary axis, i.e.,  $\lambda = +|\lambda|i$ . The stability polynomial for a general 2-stage first-order integrator is given by

$$(3.4) \quad \Phi(z) = 1 + z + kz^2,$$

where the value of the coefficient  $k$  needs to optimized so that the region enclosed by  $|\Phi(z)| \leq 1$  is maximal on the positive imaginary axis, enabling the maximal stable time step.

For the stability polynomial with purely real coefficients, i.e.,  $k \in \mathbb{R}$ , the stability condition  $|\Phi(z)| \leq 1$  on  $z = iy \in [0, iy_{\max}]$  becomes

$$(3.5) \quad (k^2y^2 + (1 - 2k))y^2 \leq 0,$$

where  $y = +|\lambda|\Delta t$ . For the integrator to be stable, we thus require  $y^2 \in [0, \frac{2k-1}{k^2}]$ . The maximal value of  $y$  is 1, which is achieved for  $k = 1$ . Hence, for real-valued integrators, the optimal stability polynomial for this system is

$$(3.6) \quad \Phi_r(z) = 1 + z + z^2$$

and the maximum stable step is  $\Delta t = \frac{1}{|\lambda_{max}|}$ .

For the stability polynomial with the complex coefficient  $k \in \mathbb{C}$ ,  $k = k_r + k_i i$ ,  $k_r, k_i \in \mathbb{R}$ , the stability condition translates to

$$(3.7) \quad (k_r^2 + k_i^2)y^2 - 2k_i y + (1 - 2k_r) =: f(y, k_r, k_i) \leq 0.$$

The stability needs to be fulfilled for vanishing  $y = 0$ , requiring that the function  $f(y, k_r, k_i) = (k_r^2 + k_i^2)y^2 - 2k_i y + (1 - 2k_r)$  needs to fulfill  $f(0, k_r, k_i) \leq 0$ , which fixes  $k_r = 1/2$ . The remaining upper root of  $f(y, k_r, k_i)$  is given by  $y = 2k_i / (\frac{1}{4} + k_i^2)$ , which attains a maximal value of 2 for  $k_i = \frac{1}{2}$ .

Thus, the optimal coefficient  $k = \frac{1}{2} + \frac{1}{2}i$  achieves a stability domain of  $y \in [0, 2]$ . Hence, the optimal stability polynomial for this system is

$$(3.8) \quad \Phi_c(z) = 1 + z + \left(\frac{1}{2} + \frac{1}{2}i\right) z^2$$

and the maximum stable step is  $\frac{2}{|\lambda_{max}|}$  which is twice as large as its real equivalent.

Similarly, if all the eigenvalues lie on the negative imaginary axis like in the case of the linear Schrodinger equation, the optimal stability polynomial is

$$(3.9) \quad \Phi_{c-}(z) = 1 + z + \left(\frac{1}{2} - \frac{1}{2}i\right) z^2$$

and the maximum stable step is also  $\frac{2}{|\lambda_{max}|}$ . ■

The stability region using complex coefficients thus covers double the length on the negative imaginary axis compared to the one obtained using purely real coefficients, enabling stable time steps twice as large as also shown in Figure 5.

The following theorem generalizes this idea further. Any first-order stability polynomial with real coefficients, for systems with eigenvalues either on the positive or negative imaginary axis, can be improved by introducing a small complex perturbation, thereby enlarging the stability region along the imaginary axis.

**Theorem 3.2.** *Consider a linear system  $\dot{y} = Ay$ , where  $y \in \mathbb{R}^n$  and  $A \in \mathbb{R}^{n \times n}$  is a matrix whose eigenvalues  $\lambda \in \mathbb{C} \setminus \mathbb{R}$  lie entirely on either the positive imaginary axis ( $\lambda = +i|\lambda|$ ) or the negative imaginary axis ( $\lambda = -i|\lambda|$ ).*

Let

$$\Phi(z) = 1 + z + \sum_{j=2}^N a_j z^j,$$

with real coefficients  $a_j \in \mathbb{R}$ , denote the stability polynomial of an  $N$ -stage (or step) first-order method. Suppose that its stability interval along the imaginary axis is  $[0, iY_R]$ , for some maximal range  $|Y_R|$ . Assume further that

$$|\Phi(iy)| < 1, \quad \forall y \in (0, Y_R).$$

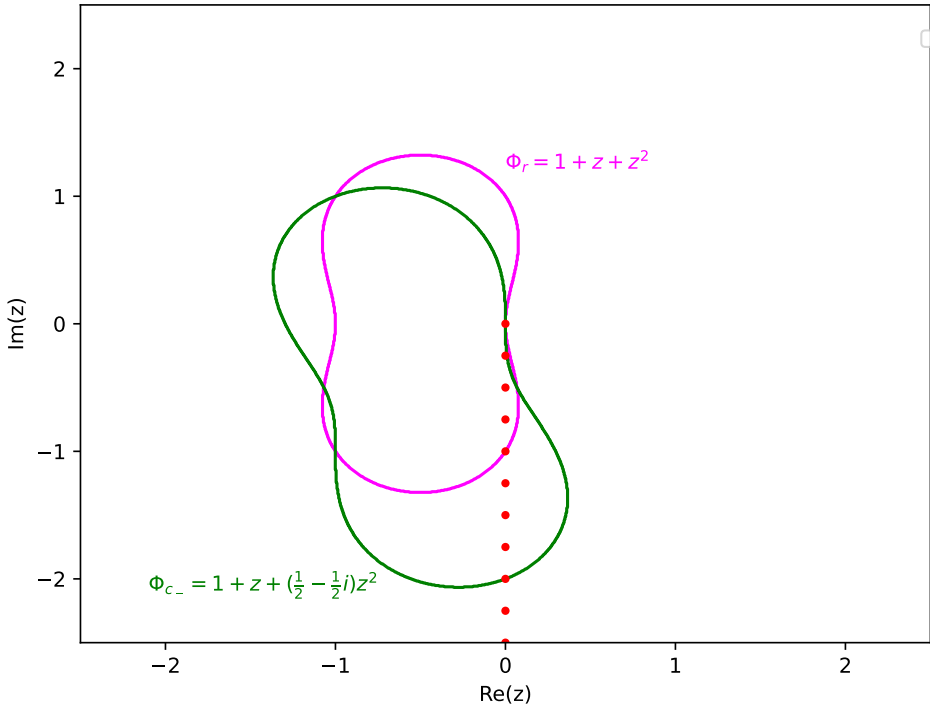


**Figure 5.** Eigenvalues of the linear Schrödinger equation lie along the negative imaginary axis (red dots). The optimal two-stage, two-step, first-order stability polynomials with real coefficients  $\Phi_r$  (Eq. 3.6, magenta) and with complex coefficients  $\Phi_{c_-}$  (Eq. 3.9, green) yield distinct stability regions. Using complex coefficients with  $\Phi_{c_-}$  expands the stability region, enabling stable time steps up to twice as large as those for the real-coefficient integrator  $\Phi_r$ .

Then, there exists a complex polynomial  $q(z)$  and a scalar  $\varepsilon > 0$  such that the perturbed polynomial

$$\Phi_\varepsilon(z) := \Phi(z) + \varepsilon q(z)$$

satisfies

$$|\Phi_\varepsilon(iy)| \leq 1, \quad \forall y \in [0, Y],$$

for some  $Y > Y_R$ . Hence, introducing complex coefficients strictly enlarges the stability region along the imaginary axis.

*Proof.* We have

$$(3.10) \quad \Phi(z) = 1 + z + a_2 z^2 + a_3 z^3 + \dots$$

The condition for stability on  $iy \in [0, iY_R]$  is  $p(y) := |\Phi(iy)|^2 \leq 1$ .

$$(3.11) \quad p(y) = |\Phi(iy)|^2 = |1 + iy + a_2(iy)^2 + a_3(iy)^3 + \dots|^2$$

$$(3.12) \quad = |(1 - a_2 y^2 + \dots) + i(y - a_3 y^3 + \dots)|^2$$

$$(3.13) \quad = (1 - a_2 y^2 + \dots)^2 + (y - a_3 y^3 + \dots)^2.$$

Since the  $a_n$  are real,  $p(y)$  can only have even powers of  $y$ .

Now consider a small complex perturbation  $\epsilon q$  to  $\Phi_\epsilon(z)$  for  $\epsilon > 0$  such that

$$(3.14) \quad \Phi_\epsilon(z) = \Phi(z) + \epsilon q(z),$$

$$(3.15) \quad p_\epsilon(y) = |\Phi_\epsilon(iy)|^2 = (\Phi(iy) + \epsilon q(iy))\overline{(\Phi(iy) + \epsilon q(iy))}$$

$$(3.16) \quad = \Phi(iy)\overline{\Phi(iy)} + \Phi(iy)\overline{\epsilon q(iy)} + \epsilon q(iy)\overline{\Phi(iy)} + \epsilon q(iy)\overline{\epsilon q(iy)},$$

$$(3.17) \quad \frac{dp_\epsilon(y)}{d\epsilon} = \Phi(iy)\overline{q(iy)} + q(iy)\overline{\Phi(iy)} + O(\epsilon) = 2\text{Real}(\Phi(iy)\overline{q(iy)}) + O(\epsilon).$$

At  $y = Y_R$ , we have that  $p(iY_R) = 1$  since  $\Phi(z)$  is optimal. This implies that  $|\Phi(iY_R)| = 1$  and  $\Phi(iY_R) = e^{i\theta}$  for some real  $\theta$ . If we pick the perturbation  $q(z) = -ie^{i\theta}z^3/Y_R^3$ , this introduces odd terms in  $p_\epsilon(y)$  according to

$$(3.18) \quad p_\epsilon(y) = p(y) + \epsilon \frac{dp_\epsilon(y)}{d\epsilon} + O(\epsilon^2)$$

$$(3.19) \quad = |\Phi(iy)|^2 - 2\epsilon \frac{y^3}{Y_R^3} \text{Real}(\Phi(iy)) + O(\epsilon^2).$$

For the interior points  $y \in (0, Y_R)$ ,  $p(y) = |\Phi(iy)|^2 < 1$ . Thus, we can pick a sufficiently small  $\epsilon$  so that  $p_\epsilon(y) \leq 1$  on  $y \in (0, Y_R)$ .

At the boundaries, we have

$$(3.20) \quad \frac{dp_\epsilon(0)}{d\epsilon} = 0, \quad \frac{dp_\epsilon(Y_R)}{d\epsilon} = -2$$

This implies that  $p_\epsilon(Y_R) < 1$  for sufficiently small  $\epsilon$ . By continuity of  $p_\epsilon(y)$  in  $y$ , there exists some  $Y > Y_R$  such that  $|\Phi_\epsilon(iy)| \leq 1$  for all  $y \in [0, Y]$ . ■

Theorems 3.1 and Theorem 3.2 demonstrate that complex time integrators constructed through the optimization of their stability regions can possess substantially larger stability domains than their real-coefficient counterparts. Consequently, optimized complex time integrators can achieve faster and more efficient time integration, as will be illustrated next.

**3.3. Numerical example: The nonlinear Schrodinger equation.** To demonstrate the practical efficiency of using the constructed complex time integrators with expanded stability regions, we consider the nonlinear Schrodinger equation.

$$(3.21) \quad iu_t + \frac{1}{2}u_{xx} + |u|^2u = 0, \quad x \in [-2\pi, 4\pi], \quad t \in [0, 6].$$

The initial condition  $u(x, 0) = u_0$  is chosen to admit the following soliton exact solution.

$$(3.22) \quad u(x, t) = \sqrt{2} \operatorname{sech}(\sqrt{2}(x - t)) e^{i(x+0.5t)}.$$

Spatial differentiation is done using the Fast Fourier Transform (FFT) with 100 modes [38, 39]. Periodic boundary conditions are imposed on the domain. This leads to a discretized system similar to the form discussed in the previous section.

We simulate the nonlinear Schrodinger equation (3.21) with the optimally stable real and complex integrators (Equations (3.6) and (3.9)) obtained in the previous subsection (see also Figure 5 again). The optimally stable real integrator advances the solution from  $y^n$  in two stages. Similar to the midpoint method, an intermediate value is first computed using a forward Euler step,

$$(3.23) \quad y^{(1)} = y^n + \Delta t F(y^n),$$

and then the solution after a time step  $\Delta t$  is updated as

$$(3.24) \quad y^{n+1} = y^n + \Delta t F(y^{(1)}),$$

where  $F(y)$  denotes the right-hand side of the nonlinear Schrödinger equation after spatial discretization. The resulting stability polynomial is given by Equation (3.6).

The optimally stable complex integrator follows a similar two-stage structure but employs a complex intermediate step.

$$(3.25) \quad y^{(1)} = y^n + \frac{(1-i)}{2} \Delta t F(y^n),$$

$$(3.26) \quad y^{n+1} = y^n + \Delta t F(y^{(1)}).$$

The resulting stability polynomial is given by Equation (3.9).

Figure 6 shows the error and computational time associated with various time steps. The optimal complex integrator (green) allows for a stable step size twice as large with even smaller error when compared to the optimal real integrator (magenta). Note that there is no additional computational effort for the complex integrator, since the Schrodinger equation already requires complex arithmetic even for a real integrator.

We show through this example that complex steps/coefficients in a time integrator can expand stability regions beyond real equivalents and allow for larger time steps. Even larger regions may be possible using methods with more stages/sub-steps, but the cost trade-off between increased evaluations and increased step size would need to be evaluated on a problem specific basis. While our primary examples have been the Schrodinger equation, they demonstrate the broader utility of complex time integration. In particular, they suggest a pathway to more efficient simulations of the complex-valued Kohn-Sham equations, and potentially other quantum systems, by exploiting asymmetric stability regions to allow larger stable time steps

**4. The Projective Integration method with complex time steps.** As mentioned earlier, the idea of sacrificing formal high-order accuracy while extending the stability region is not new. A recently popular method called Projective Integration (PI) adopts this strategy to efficiently integrate stiff systems with spectral gaps (see [18, 19, 20, 21]). In this section, we derive the first complex extensions of PI schemes and elaborate that those are ideally suited for time integration of stiff systems with complex eigenvalues and spectral gaps. We begin with an explanation of the PI method, followed by a generic example and applications.

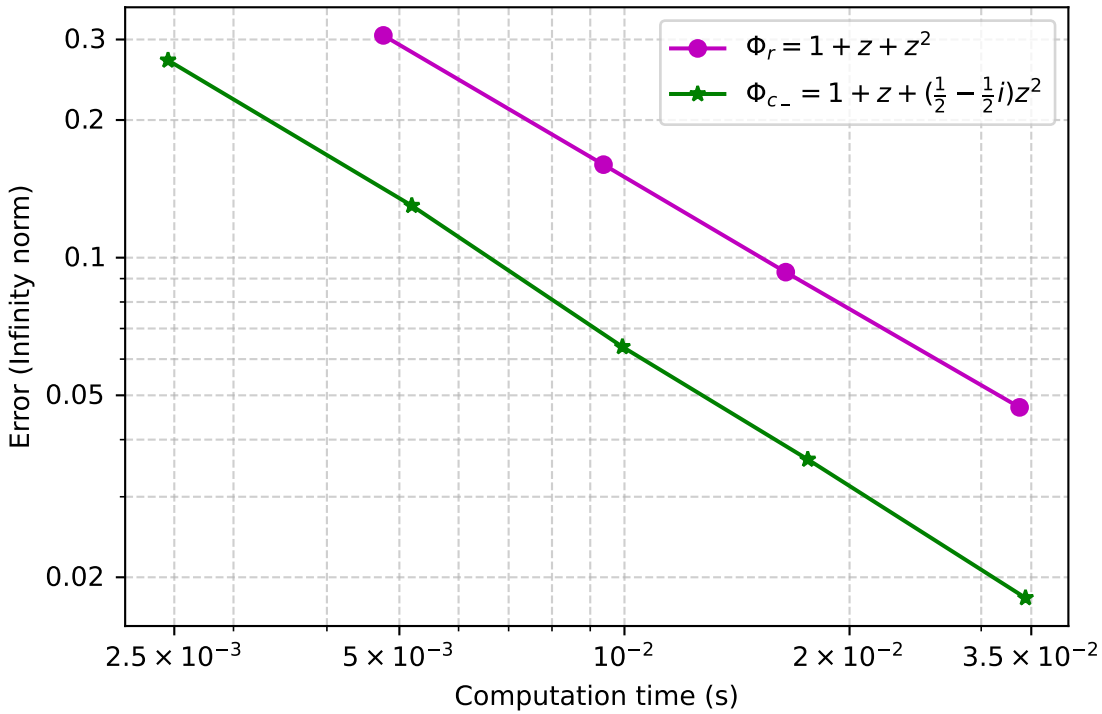


**Figure 6.** Simulation of the nonlinear Schrodinger equation (3.21) using the optimally stable 2-stage first-order real (magenta, Equation (3.6)) and complex (green, Equation (3.9)) integrators for  $\Delta t = 0.014, 0.007, 0.0035, 0.002, 0.001$ . The largest time step  $\Delta t = 0.014$  is unstable and not shown for the real integrator. Errors and computational times are averaged across 1000 runs. The complex integrator allows for twice as large stable time steps and half as much computational effort for slightly lower error.

**4.1. Projective Integration.** Projective Integration (PI) schemes are explicit schemes tailored to the stable integration of stiff ODE systems with spectral gaps. This means that they target system of the form  $\dot{y} = Ay$ , where  $y \in \mathbb{R}^n$  and  $A \in \mathbb{R}^{n \times n}$  is a matrix with two distinct clusters of eigenvalues  $\sigma_f$  and  $\sigma_s$ , representing fast and slow modes, respectively. The slow modes  $\lambda_s \in \sigma_s$  evolve on the time scale  $\mathcal{O}(1)$  and are most relevant for accuracy, but this requires the fast modes  $\lambda_f \in \sigma_f$  evolving on the short time scale  $\mathcal{O}(\epsilon)$  to be integrated in a stable manner. For traditional, explicit schemes like the FE scheme, this usually results in a prohibitively small time step  $\Delta t \approx \epsilon$ . PI methods overcome this by damping out the fast modes in a series of small (sub-)steps of size  $\delta t \approx \epsilon$  and then extrapolating the result over the remainder of a longer time step  $\Delta t$ , see [19].

A PI scheme in its simplest form utilizes a small number of  $K + 1$  small forward Euler time steps of size  $\delta t \approx \epsilon$  followed by a larger extrapolation step of the remaining time step  $\Delta t - (K + 1)\delta t$ . This is commonly referred to as the Projective Forward Euler (PFE) method,

which can be written using  $y^{n,0} = y^n$  and

$$(4.1) \quad y^{n,1} = y^{n,0} + \delta t \cdot f(y^{n,0})$$

$$(4.2) \quad y^{n,2} = y^{n,1} + \delta t \cdot f(y^{n,1})$$

$$(4.3) \quad \vdots$$

$$(4.4) \quad y^{n,K+1} = y^{n,K} + \delta t \cdot f(y^{n,K})$$

$$(4.5) \quad y^{n+1} = y^{n,K+1} + (\Delta t - (K+1)\delta t) \cdot \frac{y^{n,K+1} - y^{n,K}}{\delta t}.$$

In [40] it was recently shown that the PFE method can be written as a standard RK scheme with  $K+1$  stages using  $\Lambda := \frac{\delta t}{\Delta t}$  and the Butcher tableau given by (4.6).

$$(4.6) \quad \begin{array}{c|ccccc} 0 & 0 & & & & \\ 1 \cdot \Lambda & \Lambda & 0 & & & \\ \vdots & \vdots & \ddots & \ddots & & \\ K \cdot \Lambda & \Lambda & \dots & \Lambda & 0 & \\ \hline & \Lambda & \dots & \Lambda & 1 - K\Lambda & \end{array}$$

The stability polynomial of a PFE scheme with  $K+1$  inner steps is given by (compare [41])

$$(4.7) \quad \Phi(z) = (1 + \Lambda z)^K (1 + (1 - K\Lambda)z).$$

Up to now PI schemes have been used exclusively with real time step sizes  $\Delta t$  and  $\delta t$ . This limited their applicability to problems where the eigenvalues have small imaginary parts, as the inner integrators are typically not able to capture eigenvalues with significant imaginary parts. Allowing complex time steps opens up the possibility of larger stable time steps, extending PI methods to applications with larger imaginary eigenvalues.

In the remainder of this section, we will apply complex time stepping to PI schemes and use this to solve both real-valued and complex-valued systems.

**4.2. Complex PI schemes for a complex-valued stiff equation.** Real Forward Euler steps are typically used as the inner steps in PI schemes, while either first-order FE or higher order RK schemes are utilized for the outer steps, see [41] for high order PI schemes. If  $\Phi_{outer}$  and  $\Phi_{inner}$  denote the stability polynomials corresponding to the outer step and the inner step(s), respectively, the full stability polynomial  $\Phi_{PI}$  for a PI scheme can be expressed as as a concatenation

$$(4.8) \quad \Phi_{PI}(z) = \Phi_{inner}(z) \cdot \Phi_{outer}(z).$$

If the inner step(s) consist of  $K+1$  Forward Euler time steps with variable time step sizes  $\delta t_n = a_n \Delta t$ , then  $\Phi_{inner}$  can be written as a concatenation of these substeps.

$$(4.9) \quad \Phi_{inner}(z) = \prod_{n=1}^{K+1} (1 + a_n z).$$

The roots of  $\Phi_{inner}(z)$  are located at  $-1/a_n$ . For real time steps ( $a_n \in \mathbb{R}$ ), this results in stability regions that are centered around the negative real axis. For stiff problems where the eigenvalues contain a significant imaginary component, such stability regions centered on the real axis can lead to instability.

To illustrate this, consider the Prothero-Robinson example, a classic stiff differential equation [23], in Equation (4.10)

$$(4.10) \quad \frac{dy}{dt} = \lambda(y - \cos t) - \sin t, \quad y(0) = \frac{3}{2}.$$

For large values of  $\lambda$ , Equation (4.10) has fast transient dynamics away from its steady state solution  $y = \cos(t)$ . Although the scalar Equation (4.10) does not contain both slow and fast dynamics, it suffices as a simple example to outline the ability of complex PI schemes to capture fast dynamics for problems with non-negligible imaginary eigenvalue parts.

We now consider the complex-valued case where  $\lambda \in \mathbb{C}$  can be represented as  $\lambda = -\frac{1}{\varepsilon} + \xi i$  where  $\varepsilon \in \mathbb{R}_+$ ,  $\xi \in \mathbb{R}$  and  $\xi i$  is a small imaginary perturbation around the dominant stiff component  $-\frac{1}{\varepsilon}$ .

We solve the Prothero-Robinson equation (4.10) numerically using two different PI methods:

- (A) **Real Projective Forward Euler (PFE):** two real inner steps  $\delta t = \text{Re}(-1/\lambda)$  and the outer extrapolation step for the remainder of  $\Delta t = 0.05$ .
- (B) **Complex Projective Forward Euler (cPFE):** two complex inner steps  $\delta t = -1/\lambda$  and the outer extrapolation step for the remainder of  $\Delta t = 0.05$ .

For both schemes, given the numerical solution  $y^n$  at time  $t$ , the solution  $y^{n+1}$  at time  $t + \Delta t$  is computed via (compare (4.5))

$$(4.11) \quad y^{n,1} = y^n + \delta t \cdot f(y^n),$$

$$(4.12) \quad y^{n,2} = y^{n,1} + \delta t \cdot f(y^{n,1}),$$

$$(4.13) \quad y^{n+1} = y^{n,2} + (\Delta t - 2\delta t) \cdot \frac{y^{n,2} - y^{n,1}}{\delta t},$$

where  $f(y)$  is the right hand side of Equation (4.10). Note that (4.11) -(4.13) is equivalent to the following two-step Forward Euler update:

$$(4.14) \quad y^{n,1} = y^n + \delta t \cdot f(y^n)$$

$$(4.15) \quad y^{n+1} = y^{n,1} + (\Delta t - \delta t) \cdot f(y^{n,1}).$$

The stability diagrams for the real PFE and the complex cPFE described above as (A) and (B), respectively, are illustrated in Figure 7. We can see that the stability region of the cPFE method encompasses the complex eigenvalue  $\lambda$  while the real PFE method fails to do so. We present numerical results in Figure 8 for two representative cases:

1.  $\lambda = -10^6 + 15i$ , i.e.,  $\varepsilon = 10^{-6}$ ,  $\xi = 15$ , corresponding to a small imaginary part
2.  $\lambda = -10^6 + 20i$ , i.e.,  $\varepsilon = 10^{-6}$ ,  $\xi = 20$ , corresponding to a larger imaginary part.

In both cases, the real part of  $\lambda$  is much larger in magnitude than the imaginary part.

For  $\lambda = -10^6 + 15i$  in Figure 8 (left), the real PFE solution is oscillating but the oscillations are damped in time and the method is therefore stable. However, for only a relatively small

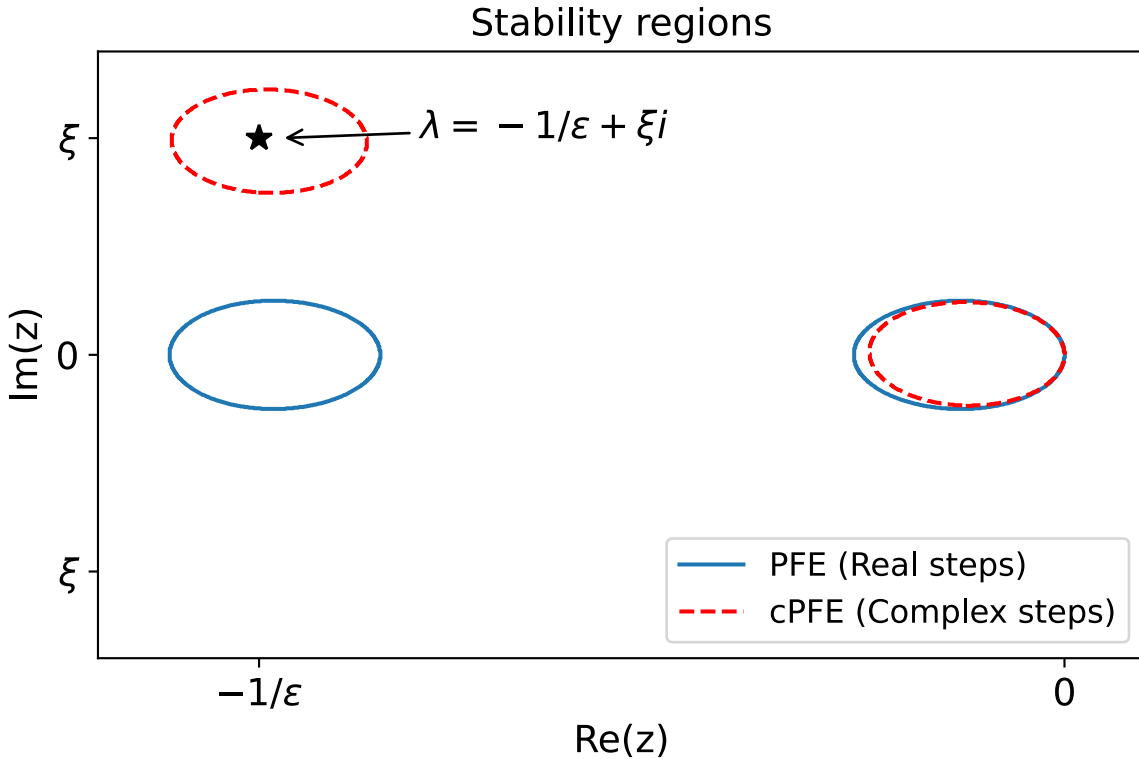


**Figure 7.** Stability regions corresponding to the real PFE method (blue) and complex cPFE method (red), together with the location of the complex eigenvalue  $\lambda$  in (4.10).

increase in the imaginary part from  $\lambda = -10^6 + 15i$  to  $\lambda = -10^6 + 20i$  in Figure 8 (right), the real PFE solution has persisting oscillations that are only semi-stable. The complex cPFE solution, however, is stable in both cases. This clearly demonstrates the benefits of complex time integration for this first example of PI schemes. However, since this example lacks a spectral gap, we next turn to a more challenging system exhibiting coupled slow and fast dynamics.

**4.3. Complex PI schemes for real-valued systems.** After the stiff scalar but complex-valued example, we now consider the two-scale, potentially stiff but real-valued system

$$(4.16) \quad \dot{y}_1 = y_2,$$

$$(4.17) \quad \dot{y}_2 = -2\mu y_2 - \omega_0^2 y_1,$$

$$(4.18) \quad \dot{y}_3 = -\lambda(y_3 - y_1).$$

The system (4.16)-(4.18) models the slow decay of a variable  $y_3$  to zero with decay rate  $\lambda \in \mathbb{R}_+$ , perturbed by the solution  $y_1$  of a damped oscillator with natural frequency  $\omega_0 \in \mathbb{R}_+$  and viscous damping coefficient  $2\mu \in \mathbb{R}_+$ . For a heavily damped system, we can write  $\mu$  as  $\mu = 1/\varepsilon$ , where  $0 < \varepsilon \ll 1$ . We further assume a highly oscillatory system where  $\omega_0^2 = 1/\varepsilon^2 + \delta^2$ , for some  $\delta > 0$ . Here, we are interested in computing a stable solution for  $y_3$  without necessarily resolving the fast dynamics of  $y_1$ .

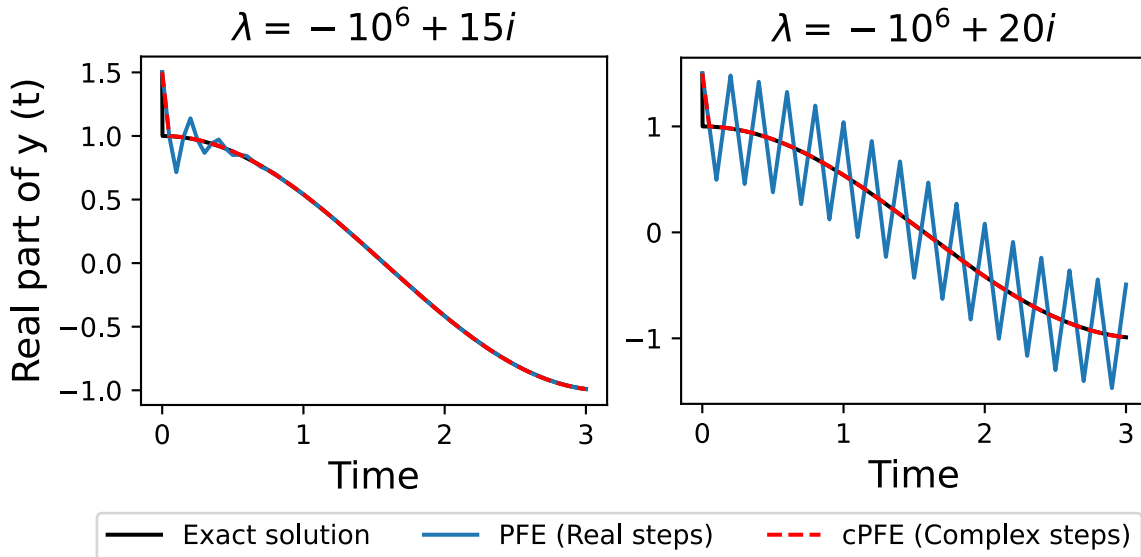


**Figure 8.** Numerical solutions of the Prothero-Robinson example (4.10) for a small imaginary component,  $\lambda = -10^6 + 15i$  (left), and a larger imaginary component,  $\lambda = -10^6 + 20i$  (right). The exact solution is shown in black, the real PFE in blue, and the complex cPFE in dashed red. The complex cPFE method remains stable and free of oscillations in both cases due to its stability region being shifted off the real axis, allowing it to capture the complex eigenvalue  $\lambda$ .

System (4.16)-(4.18) can be written as the linear system

$$(4.19) \quad \begin{pmatrix} \dot{y}_1 \\ \dot{y}_2 \\ \dot{y}_3 \end{pmatrix} = \underbrace{\begin{pmatrix} 0 & 1 & 0 \\ -1/\varepsilon^2 - \delta^2 & -2/\varepsilon & 0 \\ \lambda & 0 & -\lambda \end{pmatrix}}_A \begin{pmatrix} y_1 \\ y_2 \\ y_3 \end{pmatrix},$$

where the system matrix  $A \in \mathbb{R}^{3 \times 3}$  has eigenvalues

$$(4.20) \quad \lambda \in \sigma(A) = \left\{ -\lambda, -\frac{1}{\varepsilon} + i\delta, -\frac{1}{\varepsilon} - i\delta \right\},$$

thus resulting in two complex conjugated eigenvalues.

For  $\lambda \ll 1/\varepsilon$ , the system is stiff, with scale separation between the fast oscillatory movement of  $y_1$  and the slow decay of  $y_3$  as illustrated in Figure 9 (right). We consider the parameters  $\lambda = 1, \varepsilon = 0.1, \delta = 22.913$  with the initial conditions  $(y_1, y_2, y_3) = (4, 2, 5)$ . The eigenvalues are shown as black dots in Figure 9 (left), together with the stability region of the real PI method (blue), and the stability region of the complex PI method (red). Both methods use two inner evaluations of the right-hand side (Equation (4.19)) with inner step size  $\delta t$ . For the real PI method,  $\delta t = 1/(-\frac{1}{\varepsilon})$ , while for the complex PI method,  $\delta t = 1/(-\frac{1}{\varepsilon} \pm i\delta)$ . The real PI stability region includes only a narrow region around the imaginary axis while the complex PI stability region encompasses the complex eigenvalues. This means that a real PI method would lead to unstable numerical simulations for this application, while the complex PI method is stable by construction.

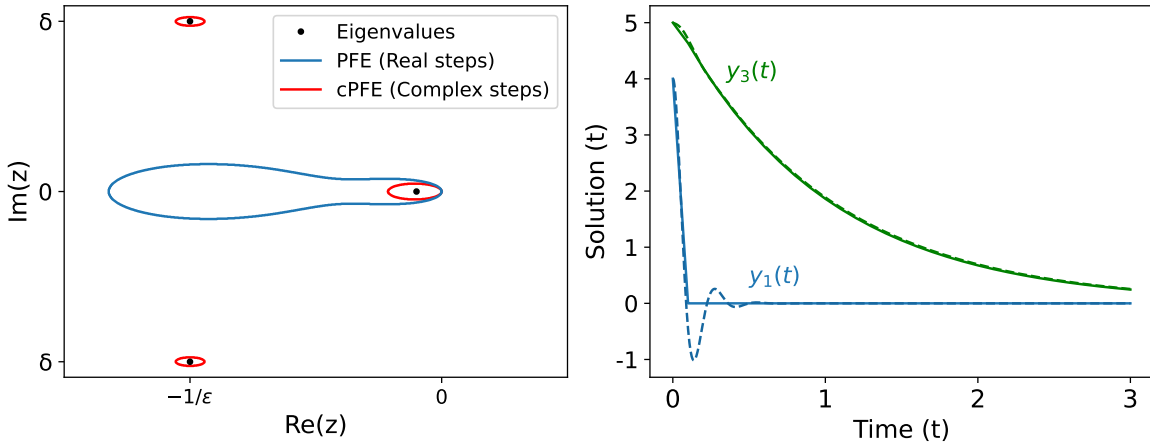


**Figure 9.** Left: Spectrum of the system (4.19), consisting of one real eigenvalue associated with slow decay and a pair of complex conjugate eigenvalues modeling fast oscillatory dynamics. The stability region of the complex cPFE method (red) encloses all eigenvalues, while the real PFE stability region (blue) fails to capture the oscillatory modes. Right: Time evolution of (4.18)–(4.18) for parameters  $\lambda = 1, \varepsilon = 0.1, \delta = 22.913$  with the initial conditions  $(y_1, y_2, y_3) = (4, 2, 5)$ .  $y_3$  is influenced by the oscillations of  $y_1$  in the beginning, but  $y_1$  quickly gets damped to 0, then  $y_3$  slowly decays further. Dashed lines indicate the exact solution, while solid lines show the numerical solution obtained using the stable cPFE method (the real PFE method is unstable at this step size). The outer step is  $\Delta t = 0.1$  with two complex inner steps  $\delta t = 1/(-\frac{1}{\varepsilon} \pm i\delta)$ .

This example has been constructed to reflect the regime in which PI is intended to be used. The system exhibits a clear spectral gap, with a slow mode associated with the real eigenvalue  $-\lambda$  and fast modes associated with eigenvalues of large negative real part and non-negligible imaginary component. In PI, the outer time step is chosen according to the slow time scale of interest, while the role of the inner steps is to stabilize the fast dynamics. Consequently, we select  $\Delta t \approx \mathcal{O}(\frac{1}{\lambda})$  corresponding to the slow decay rate, and do not adjust this outer step to accommodate stability restrictions imposed by the fast modes. At this slow-scale step size, a real PI scheme becomes unstable due to the oscillatory fast eigenvalues, whereas a complex PI scheme remains stable by appropriately shifting the stability region.

A stable real PI or real Forward Euler method is technically possible, but would require a much smaller time step, e.g.,  $\Delta t = 1/\| -\frac{1}{\varepsilon} + i\delta \|$  in case of the explicit Euler method. Such a choice would force the method to resolve the fast dynamics and negate the computational advantage that PI is designed to provide. In contrast, for a complex PI scheme, a large outer time step can simply be chosen as  $\Delta t = \frac{1}{\lambda}$  and the inner time step should be  $\delta t = 1/(-\frac{1}{\varepsilon} + i\delta)$  including a complex part that allows to capture the complex eigenvalues. This results in a stable and efficient numerical solution as shown in Figure 9 (right).

**5. Discussion.** This paper explores the benefits of leaving the real line for the numerical time integration of stiff problems. We show analytically and numerically that complex time stepping can be used to expand stability regions, allowing larger, stable time steps. Expanded stability regions have been previously designed using Runge-Kutta methods [24, 28], but

we show that complex coefficients in the optimal stability polynomial allow for even larger stability regions, particularly for systems with complex-valued spectra.

The fact that the stability region can be increased by changing the integration domain rather than the integration method may also be appealing in scenarios where particular integrators with specific properties (such as nonlinear stability) for specific differential equations are desired. Although our analysis is restricted to linear stability, the numerical results for the nonlinear Schrodinger equation suggest that complex time-stepping strategies can be effective in nonlinear settings as well. This observation points toward the possibility that complex integrators could satisfy nonlinear stability guarantees such as Strong Stability Preserving properties [42, 43], although establishing such guarantees lies beyond the scope of the present work.

We intend this paper to be an introduction to and initiation of the search for efficient time integrators that take advantage of paths in the complex plane. For simulating quantum systems with inherently complex-valued equations [36], complex integrators allow for expanded stability regions at minimal computational cost, making it a particularly promising application of our method. We have mostly focused on creating integrators with improved stability, but many other desirable properties including energy and momentum preservation, remain to be explored. The complex plane offers an extra dimension on which any integrator can be improved, opening up a new realm of possibilities when designing time-stepping methods.

**6. Acknowledgements.** We would like to thank Emil Constantinescu, David Ketcheson, Alvin Bayliss and David Chopp for extensive feedback and valuable suggestions.

## REFERENCES

- [1] James Ward Brown and Ruel V Churchill. *Complex variables and applications eighth edition*. McGraw-Hill Book Company, 2009.
- [2] Norman S Nise. *Control systems engineering*. John Wiley & Sons, 2020.
- [3] George F Corliss. Integrating odes in the complex plane—pole vaulting. *Mathematics of Computation*, 35(152):1181–1189, 1980.
- [4] JE Chambers. Symplectic integrators with complex time steps. *The Astronomical Journal*, 126(2):1119, 2003.
- [5] Sergio Blanes, Fernando Casas, and Ander Murua. Splitting methods for differential equations. *Acta Numerica*, 33:1–161, 2024.
- [6] Sergio Blanes, Fernando Casas, and Alejandro Escorihuela-Tomàs. Applying splitting methods with complex coefficients to the numerical integration of unitary problems. *Journal of Computational Dynamics*, 9(2):85–101, 2022.
- [7] François Castella, Philippe Chartier, Stéphane Descombes, and Gilles Vilmart. Splitting methods with complex times for parabolic equations. *BIT Numerical Mathematics*, 49(3):487–508, 2009.
- [8] Winfried Auzinger, Harald Hofstätter, David Ketcheson, and Othmar Koch. Practical splitting methods for the adaptive integration of nonlinear evolution equations. part i: Construction of optimized schemes and pairs of schemes. *BIT Numerical Mathematics*, 57(1):55–74, 2017.
- [9] Fernando Casas, Philippe Chartier, Alejandro Escorihuela-Tomàs, and Yong Zhang. Compositions of pseudo-symmetric integrators with complex coefficients for the numerical integration of differential equations. *Journal of Computational and Applied Mathematics*, 381:113006, 2021.
- [10] Sergio Blanes, Fernando Casas, and Ander Murua. Splitting methods with complex coefficients. *SeMA Journal*, 50(1):47–60, 2010.
- [11] Eskil Hansen and Alexander Ostermann. High order splitting methods for analytic semigroups exist. *BIT Numerical Mathematics*, 49(3):527–542, 2009.

[12] Fernando Casas and Alejandro Escorihuela-Tomàs. High order integrators obtained by linear combinations of symmetric-conjugate compositions. *Applied Mathematics and Computation*, 414:126700, 2022.

[13] Thorsten Orendt, Jürgen Richter-Gebert, and Michael Schmid. Geometry of numerical complex time integration. *arXiv preprint arXiv:0903.1585*, 2009.

[14] Denis M Filatov. On complex-stepped Runge-Kutta methods for exact time integration of linear PDEs. *HAIT Journal of Science and Engineering C*, 4:1–2, 2006.

[15] Alexander Borisovich Al'shin, Elena Alexandronva Al'shina, Nikolai Nikolaevich Kalitkin, and AB Koryagina. Rosenbrock schemes with complex coefficients for stiff and differential algebraic systems. *Computational Mathematics and Mathematical Physics*, 46(8):1320–1340, 2006.

[16] Tommaso Buvoli and Mayya Tokman. Constructing new time integrators using interpolating polynomials. *SIAM Journal on Scientific Computing*, 41(5):A2911–A2937, 2019.

[17] Jithin D George, Samuel Y Jung, and Niall M Mangan. Walking into the complex plane to “order” better time integrators. *arXiv preprint arXiv:2110.04402*, 2021.

[18] John Maclean and Georg A Gottwald. On convergence of higher order schemes for the projective integration method for stiff ordinary differential equations. *Journal of Computational and Applied Mathematics*, 288:44–69, 2015.

[19] C William Gear and Ioannis G Kevrekidis. Projective methods for stiff differential equations: problems with gaps in their eigenvalue spectrum. *SIAM Journal on Scientific Computing*, 24(4):1091–1106, 2003.

[20] Ward Melis, Thomas Rey, and Giovanni Samaey. Projective and telescopic projective integration for the nonlinear BGK and Boltzmann equations. *The SMAI journal of computational mathematics*, 5:53–88, 2019.

[21] Julian Koellermeier and Giovanni Samaey. Projective integration schemes for hyperbolic moment equations. *Kinetic and Related Models*, 14(2):353–387, 2021.

[22] Ernst Hairer, Syvert P Nørsett, and Gerhard Wanner. *Solving ordinary differential equations. 1, Nonstiff problems*. Springer-Vlg, 1993.

[23] Randall J LeVeque. *Finite difference methods for ordinary and partial differential equations: steady-state and time-dependent problems*. SIAM, 2007.

[24] W Riha. Optimal stability polynomials. *Computing*, 9(1):37–43, 1972.

[25] J Douglas Lawson. An order five runge-kutta process with extended region of stability. *SIAM Journal on Numerical Analysis*, 3(4):593–597, 1966.

[26] Assyr Abdulle. On roots and error constants of optimal stability polynomials. *BIT Numerical Mathematics*, 40(1):177–182, 2000.

[27] Andrei Bogatyrev. Effective computation of optimal stability polynomials. *Calcolo*, 41(4):247–256, 2004.

[28] David Ketcheson and Aron Ahmadia. Optimal stability polynomials for numerical integration of initial value problems. *Communications in Applied Mathematics and Computational Science*, 7(2):247–271, 2013.

[29] Matteo Parsani, David I Ketcheson, and W Deconinck. Optimized explicit runge–kutta schemes for the spectral difference method applied to wave propagation problems. *SIAM Journal on Scientific Computing*, 35(2):A957–A986, 2013.

[30] Ethan J Kubatko, Benjamin A Yeager, and David I Ketcheson. Optimal strong-stability-preserving runge–kutta time discretizations for discontinuous galerkin methods. *Journal of Scientific Computing*, 60(2):313–344, 2014.

[31] David I Ketcheson, Matteo Parsani, Zachary Grant, Aron Ahmadia, and Hendrik Ranocha. Rk-opt: A package for the design of numerical ode solvers. 2020.

[32] David I Ketcheson, Hendrik Ranocha, Matteo Parsani, Umair bin Waheed, and Yiannis Hadjimichael. Nodepy: A package for the analysis of numerical ode solvers. 2020.

[33] Kisung Kang, Alina Kononov, Cheng-Wei Lee, Joshua A Leveillee, Ethan P Shapera, Xiao Zhang, and André Schleife. Pushing the frontiers of modeling excited electronic states and dynamics to accelerate materials engineering and design. *Computational Materials Science*, 160:207–216, 2019.

[34] Dong An and Lin Lin. Quantum dynamics with the parallel transport gauge. *Multiscale Modeling & Simulation*, 18(2):612–645, 2020.

[35] Dong An, Di Fang, and Lin Lin. Parallel transport dynamics for mixed quantum states with applications to time-dependent density functional theory. *Journal of Computational Physics*, 451:110850, 2022.

- [36] Alina Kononov, Cheng-Wei Lee, Tatiane Pereira dos Santos, Brian Robinson, Yifan Yao, Yi Yao, Xavier Andrade, Andrew David Baczewski, Emil Constantinescu, Alfredo A Correa, et al. Electron dynamics in extended systems within real-time time-dependent density-functional theory. *MRS communications*, 12(6):1002–1014, 2022.
- [37] Jun John Sakurai and Jim Napolitano. *Modern quantum mechanics*. Cambridge University Press, 2020.
- [38] Lloyd N Trefethen. *Spectral methods in MATLAB*. SIAM, 2000.
- [39] Bengt Fornberg. *A practical guide to pseudospectral methods*, volume 1. Cambridge university press, 1998.
- [40] Julian Koellermeier and Giovanni Samaey. Projective integration methods in the runge–kutta framework and the extension to adaptivity in time. *Journal of Computational and Applied Mathematics*, 454:116147, 2025.
- [41] Pauline Lafitte, Annelies Lejon, and Giovanni Samaey. A High-Order Asymptotic-Preserving Scheme for Kinetic Equations Using Projective Integration. *SIAM Journal on Numerical Analysis*, 54(1):1–33, January 2016.
- [42] Sigal Gottlieb, Chi-Wang Shu, and Eitan Tadmor. Strong stability-preserving high-order time discretization methods. *SIAM review*, 43(1):89–112, 2001.
- [43] Sigal Gottlieb, David I Ketcheson, and Chi-Wang Shu. High order strong stability preserving time discretizations. *Journal of Scientific Computing*, 38(3):251–289, 2009.